Information theory based design of phase-change memories

Michele Franceschini, L. A. Lastras-Montaño, John P. Karidis, Ashish Jagmohan
IBM T.J. Watson Research Center
1101 Kitchawan road, Yorktown Heights, NY, USA
email: {franceschini,lastrasl,karidis,ashishja}@us.ibm.com

***Abstract*—Due to the high device density and the advent of multiple bits per cell, modern nonvolatile memories are characterized by a non-deterministic behavior. We focus on phase-change memory (PCM), whose memory cell can be seen as a programmable resistor, and use information theory tools to investigate how the cell structure influences the storage capacity of this memory technology. In particular, we numerically compute the storage capacity of two known cell structures, i.e., the series cell, and the parallel cell. The results suggest that, in practical scenarios, the parallel cell structure is characterized by significantly larger storage capacity.**

I. Introduction

Phase-change memory (PCM) is an emerging memory technology that uses the property of some phase change materials, usually chalcogenide glasses, to exist in two practically stable phases, i.e., amorphous and polycrystalline, characterized by significantly different electrical properties [1]. A PCM cell usually contains a volume of phase-change material and electrical contacts that allow to program and read the memory cell. The phase distribution is controlled by applying specific electrical programming pulses that in turn influence the internal temperature profile of the cell thus allowing to control the phase distribution. Typically, since a PCM cell behaves as a programmable resistor, the information is stored in a PCM cell as a resistance value. Although in the past, both academic and industrial research focused on the development of binary PCM cells, exploiting the capability of the material to switch from a low to an high resistivity whose values differ by 3 orders of magnitude [1], more recently, there has been increasing interest in multiple-bit-per-cell schemes [2]–[4]. Multi-bit PCM is achieved by accurately controlling the PCM cell resistance, usually by means of a write-and-verify programming scheme [2]–[4].

Although there are several sources of non ideality affecting PCM memory arrays, a peculiar characteristic of PCM is that the amorphous phase appears to be characterized by noisy electrical parameters [5]. This suggests to model PCM as a communications channel [6], whose fundamental parameter is the so-called *storage capacity*, i.e., the maximum average number of bits per cell that can be reliably stored in the device.

Currently the design criteria for PCM are mostly based, either directly or indirectly, on a threshold based decision scheme for binary cells, which mostly leads to the maximization of the *contrast ratio*, i.e., the ratio between the high resistance state, also known as the *reset state*, and the and the low resistance state, or *set state* [1].

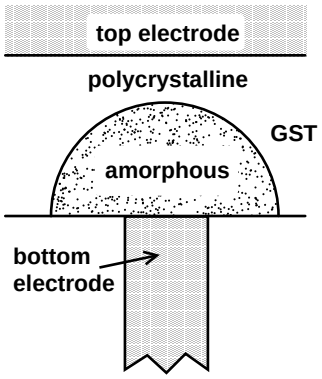

Fig. 1. Common PCM cell structure known as mushroom cell.

In this paper, we consider storage capacity as a design criterion for PCM cells. In particular, we investigate, with reference to a 2D cell model, how storage capacity is influenced by the geometrical distribution of amorphous material in the PCM cell, which in turn is influenced by the physical cell design itself. First we analyze two different cell paradigms: the *series cell*, in which most of the current paths pass through amorphous material, and the *parallel cell*, in which most of the current paths pass through polycrystalline material, and demonstrate the superiority of the parallel paradigm. Then, we numerically investigate a larger space of geometrical distributions of the amorphous material obtaining insights on what should be the programming capabilities of the PCM cell.

The paper is structured as follows. In Section II, preliminaries on PCM are given. In Section III, a simplified 2D cell model is described. In Section IV, the series and parallel cell model are analyzed and providing for each case an equivalent additive channel model. In Section V, the storage capacity is investigated using a more general input distribution space. Section VI concludes the paper.

II. Phase-Change Memory Preliminaries

A. Basic Cell Structure and Operation

A typical phase-change memory cell consists of two electrodes contacting an amount of phase change material. The most common family of phase-change material are the chalcogenide glasses, and, in particular those containing mostly Ge,

Sb, and Te elements (GST). Figure 1 illustrates a common cell structure, known as *mushroom cell* [1]. This cell consists of a thin bottom electrode covered by a blanket of GST material which is contacted at the top by a conductive layer that acts as top electrode. As mentioned above, the phase change material can exist in two practically stable phases, a crystalline one, characterized by relatively low resistivity, and an amorphous one, characterized by a resistivity orders of magnitude (3 are not uncommon) higher than that of the crystalline phase [1]. By applying a sufficiently large electrical signal to the cell, the GST material close to the bottom electrode contact can be heated and if the temperature reaches the melting temperature (~ 600C), a molten mass can be created. An abrupt reduction in temperature, obtained by a sudden removal of the electrical signal, quenches the molten material, thus creating amorphous GST. The amorphous material naturally tends to recrystallize, however the speed of the phenomenon is appreciable only at temperatures close to the so called crystallization temperature (~ 300C). Therefore, to recrystallize the amorphous material, an electrical signal which is capable of heating the cell to a temperature close to the crystallization temperature, yet lower than the melting temperature, is applied to the cell. The operation of creating amorphous material is commonly termed *reset operation*, whereas, the operation of recrystallizing the cell, is known as *set operation*. To read the memory cell, a small fixed voltage is applied to the cell and the current flowing through the cell is measured, thus allowing an estimate of the resistance of the memory cell.

B. Non-idealities

There are several parameters influencing the capability of PCM of storing information. Among these are

- variability of the geometry of the cell and the chemical composition of the phase change material;
- non-deterministic programming behavior;
- noisiness of the electrical parameters.

The first point is expected to improve as the technology becomes more mature. The second point, i.e., non-deterministic outcome of a programming operation, can be described as a noise, a *write noise*. The recently introduced theory of rewritable channels [7] investigates the relationship between programming algorithms and the amount of information that can be stored in average in a rewritable memory cell such as a PCM cell. The third point, namely, the fact that the electrical parameters of the phase-change material are noisy, is the focus of this paper. In particular, it has been shown, both empirically and through analytical modeling, how the electrical behavior of the amorphous phase of a phase-change material is driven by random processes [5], [8]. In [6], the logarithm of the resistance of a PCM cell has been described as a Wiener process with drift (in logarithmic time). On the other hand, it is reasonable to expect the crystalline phase to be almost noiseless, given its stable nature (see, e.g., [6], or [9, Fig. 6]). Based on these simple observations, i.e., the amorphous material is noisy, the crystalline material is stable, in the following sections, we will investigate how the geometrical distribution of amorphous material influences the capability of a cell to store data.

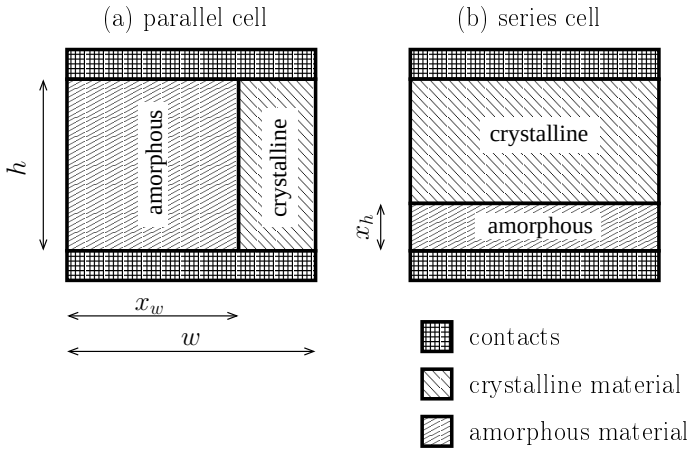

Fig. 2. 2D models for parallel (a) and series (b) cells.

III. Simplified 2D Models for Series and Parallel Cells

The mushroom cell in Fig. 1 has a peculiarity: whenever there is a non-negligible presence of amorphous material on top of the bottom electrode, all the current that passes through the cell must flow through the amorphous material. In other words, in every current path, there is amorphous material in series with crystalline material. This can be abstracted into the concept of the *series cell*, formed by two layers, one of amorphous material and the other of crystalline material. The cell is programmed by changing the thickness of the amorphous material while keeping constant the total thickness of the phase-change material. This simple abstract model has been described in [10], together with its dual concept, i.e., the *parallel cell*, where amorphous and crystalline material are connected in parallel, thus always providing a current path through the crystalline material.

The series and parallel model can be, without loss of generality, investigated in a two-dimensional domain. In Figure 2, simplified 2D models for a parallel cell (a) and a series cell (b) are shown. Both cells are rectangular patches of (two-dimensional) phase-change material of width w and height h, with electrical contacts at the top and the bottom. The series cell is programmed by controlling the thickness x_h of the amorphous material whereas the parallel cell is programmed by controlling the thickness x_w. We assume that the surface resistivity of the crystalline material ρ_c is known, whereas the surface resistivity of the amorphous material ρ_a is a random variable with known distribution $f_{\rho_a}(\rho_a)$. The total resistance of the two cells is given by

$$r_{\text{ser}} = \rho_a \frac{x_h}{w} + \rho_c \frac{h - x_h}{w} \quad (1)$$

$$r_{\text{par}} = \left(\frac{1}{\rho_a} \frac{x_w}{h} + \frac{1}{\rho_c} \frac{w - x_w}{h} \right)^{-1} \quad (2)$$

where $r_{\rm ser}$ and $r_{\rm par}$ denote the resistance of the series and parallel cell, respectively.

Intuitively, the two configurations are particularly interesting due to the large difference in resistivity of the amorphous and crystalline material. In particular, any structure characterized by the presence of a conductive path between the two electrodes entirely occupied by crystalline material, will exhibit a behavior similar to that of the parallel cell. In fact, since the resistivity of the amorphous material is often more than two orders of magnitude larger than that of the crystalline one, whenever a path through only crystalline material exists, the current will crowd into it, avoiding the passage through the amorphous material.

IV. Parallel and Series Structure Analysis

In the following we will show that, assuming perfect control at programming time of x_w and x_h, both parallel and series cells are equivalent to an additive noise channel, regardless of the distribution of ρ_a. Moreover we will show that in both cases, the capability of setting x_h or x_w to arbitrarily low values leads to an infinite capacity, whereas if x_h and x_w are lower bounded by a positive quantity, numerical analysis shows that the parallel cell has significantly better performance that the series cell.

A. Equivalent Additive Noise Channels

In the following we will assume that $P(\rho_a \leq \rho_c) = 0$. This assumption is well supported by experimental results (the typical value of ρ_a is 2 to 4 orders of magnitude larger than ρ_c)[1].

To prove that the series channel is equivalent to an additive noise channel we start from (1) and write

$$\begin{aligned} r_{\rm ser} &= \rho_a \frac{x_h}{w} + \rho_c \frac{h - x_h}{w} && (3)\\ r_{\rm ser} w &= \rho_a x_h + \rho_c (h - x_h) && (4)\\ r_{\rm ser} \frac{w}{\rho_c h} &= \frac{\rho_a}{\rho_c}\frac{x_h}{h} + 1 - \frac{x_h}{h} && (5)\\ \log\left(r_{\rm ser}\frac{w}{\rho_c h} - 1\right) &= \log\left(\frac{\rho_a}{\rho_c} - 1\right) + \log\frac{x_h}{h}\,. && (6) \end{aligned}$$

Now, let us define

$$\begin{aligned} \xi_{\rm ser} &= \log\frac{x_h}{h} && (7)\\ y_{\rm ser} &= \log\left(r_{\rm ser}\frac{w}{\rho_c h} - 1\right) && (8)\\ w_{\rm ser} &= \log\left(\frac{\rho_a}{\rho_c} - 1\right)\,. && (9) \end{aligned}$$

Since $\xi_{\rm ser}$ is a deterministic invertible function of x_h and $y_{\rm ser}$ is a deterministic invertible function of $r_{\rm ser}$, we have that $I(X_h; R_{\rm ser}) = I(\Xi_{\rm ser}; \Xi_{\rm ser} + W_{\rm ser}) = I(\Xi_{\rm ser}; Y_{\rm ser})$ for all distributions on X_h and ρ_a for which $I(X_h; R_{\rm ser})$ can be computed and for which $P(\rho_a \leq \rho_c) = 0$, which guarantees the invertibility of $y_{\rm ser}(r_{\rm ser})$.

[1]See, e.g., [3, Fig. 3].

Similarly for the parallel cell model,

$$\begin{aligned} r_{\rm par} &= \left(\frac{1}{\rho_a}\frac{x_w}{h} + \frac{1}{\rho_c}\frac{w - x_w}{h}\right)^{-1} && (10)\\ \frac{h\rho_c}{w r_{\rm par}} &= \frac{\rho_c}{\rho_a}\frac{x_w}{w} + 1 - \frac{x_w}{w} && (11)\\ \log\left(1 - \frac{h\rho_c}{w r_{\rm par}}\right) &= \log\left(1 - \frac{\rho_c}{\rho_a}\right) + \log\frac{x_w}{w} && (12) \end{aligned}$$

With the following definitions

$$\begin{aligned} \xi_{\rm par} &= \log\frac{x_w}{w} && (13)\\ y_{\rm par} &= \log\left(1 - \frac{h\rho_c}{w r_{\rm par}}\right) && (14)\\ w_{\rm par} &= \log\left(1 - \frac{\rho_c}{\rho_a}\right) && (15) \end{aligned}$$

we have that $I(X_w; R_{\rm par}) = I(\Xi_{\rm par}; \Xi_{\rm par} + W_{\rm par}) = I(\Xi_{\rm par}; Y_{\rm par})$ for all distributions on X_w and ρ_a for which $I(X_w; R_{\rm par})$ can be computed and for which $P(\rho_a \leq \rho_c) = 0$.

Let us assume that the only constraint on the written x_h or x_w values is given by the support of attainable values, i.e., $x_h, x_w \in [x_{\min}, x_{\max}]$. The corresponding input distribution constraint in the equivalent series and parallel channels are

$$\begin{aligned} \xi_{\rm ser} &\in [\log\frac{x_{\min}}{h}, \log\frac{x_{\max}}{h}] && (16)\\ \xi_{\rm par} &\in [\log\frac{x_{\min}}{w}, \log\frac{x_{\max}}{w}]\,. && (17) \end{aligned}$$

If $x_{\min} = 0$ the measure of the domain of the input variable becomes infinite. If W has a differential entropy, this leads to an infinite capacity. In order to show this, we observe that, using a uniform distribution between $[\min\xi_{\rm ser}, \max\xi_{\rm ser}]$ for $\Xi_{\rm ser}$ (or, similarly, $[\min\xi_{\rm par}, \max\xi_{\rm par}]$ for $\Xi_{\rm par}$) yields $h(\Xi_{\rm ser}) = \log(\max\xi_{\rm ser} - \min\xi_{\rm ser})$ (or $h(\Xi_{\rm par}) = \log(\max\xi_{\rm par} - \min\xi_{\rm par})$). Observe that

$$\begin{aligned} I(\Xi; Y) &= I(\Xi; \Xi + W) && (18)\\ &= h(\Xi) - h(\Xi|Y) && (19)\\ &= h(\Xi) - h(Y - \Xi|Y) && (20)\\ &= h(\Xi) - h(W|Y) && (21)\\ &\geq h(\Xi) - h(W) && (22)\\ &= \log(\max\xi_{\rm ser} - \min\xi_{\rm ser}) - h(W_{\rm ser}) \quad \text{(series)} && (23)\\ &= \log(\max\xi_{\rm par} - \min\xi_{\rm par}) - h(W_{\rm par}) \quad \text{(parallel)} && (24) \end{aligned}$$

We have that the storage capacity as a function of the extremes of the geometric parameter x_h (or x_w, for the parallel case) $C(x_{\max}, x_{\min})$ is lower bounded by $\log(\log x_{\max}/h - \log x_{\min}/h) - h(W_{\rm ser})$ (or $\log(\log x_{\max}/w - \log x_{\min}/w) - h(W_{\rm par})$, in the parallel case), therefore, since $h(W_{\rm ser})$ and $h(W_{\rm par})$ do not depend on the distribution of $\Xi_{\rm ser}$ and $\Xi_{\rm par}$, respectively,

$$\lim_{x_{\min}\to\infty} C(x_{\max}, x_{\min}) = \infty\,.$$

We remark that, one $x_{\max}$ is fixed, the above lower bound on capacity grows as $\log\log x_{\min}/h$ (or $\log\log x_{\min}/w$ in the

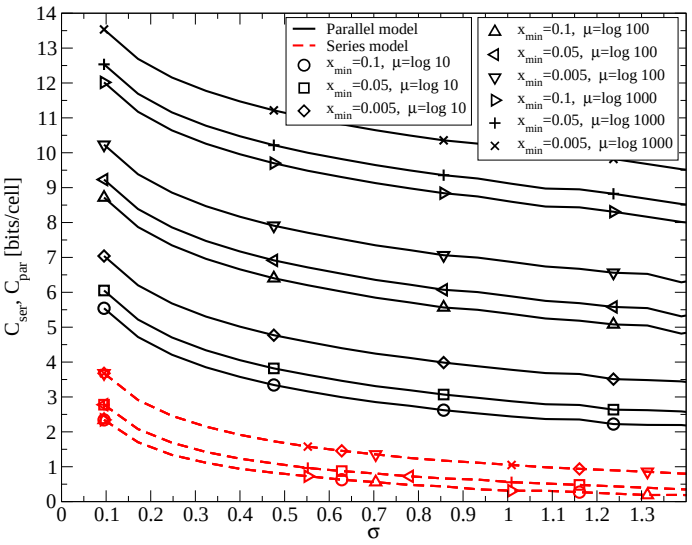

Fig. 3. Capacity versus noise variance.

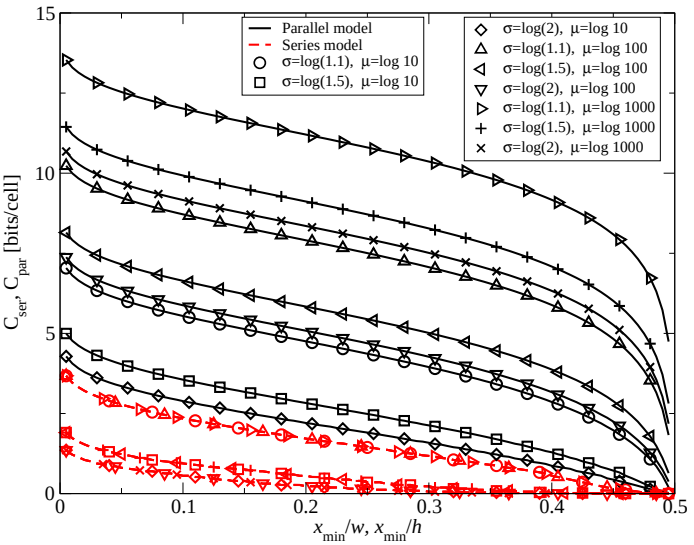

Fig. 4. Capacity versus minimum amorphous material thickness.

parallel case). It is also possible to show that, asymptotically, the capacity is also upper bounded by a $\log\log(\cdot)$ type growth (e.g., using the general upper bound for peak input constraint in [11]).

B. Numerical Observations

From a practical stand point, ρ_a will be always significantly larger than ρ_c. Moreover, it is reasonable to expect w and h to be of the same order of magnitude. Given these considerations, one can observe that the equivalent series cell noise $W_{\rm ser}$ in (9) can be approximated by ($P(\rho_a \gg \rho_c) \simeq 1$)

$$W_{\rm ser} \simeq \log \frac{\rho_a}{\rho_c}\,.$$

On the other hand

$$W_{\rm par} \simeq -\frac{\rho_c}{\rho_a}$$

which clearly entails a very small noise (i.e., $|W_{\rm par}| \ll 1$).

Following [6], we assume a normal distribution of the logarithmic resistance of the reset state. This implies assuming a log-normal distribution for the resistivity of the amorphous material. To ensure the condition $P(\rho_a \leq \rho_c) = 0$, we shift the distribution by ρ_c, which, for any practical purposes is a negligible amount. The distribution is therefore

$$f_{\rho_a}(\rho_a) = \begin{cases} \frac{1}{(\rho_a-\rho_c)\sigma\sqrt{2\pi}} e^{-\frac{(\log(\rho_a-\rho_c)-\mu)^2}{2\sigma^2}} & \text{if } \rho_a > \rho_c \\ 0 & \text{elsewhere} \end{cases}$$

where μ is the average of the logarithm of ρ_a and σ is the standard deviation of the logarithm of ρ_a.

To compute storage capacity values we quantize the equivalent channel input and output and use the Blahut-Arimoto [12] algorithm. The quantization granularity has been increased until numerical convergence was observed. From the equations in Section IV-A, it is clear that the mutual information of the series channel does not depend on w and similarly, that of the parallel channel does not depend on h. Moreover, multiplying x_h and h, or x_w and w, and ρ_a and ρ_c by a common factor does not change the mutual information. Therefore without loss of generality we can assume $\rho_c = 1$ and $w = h = 1$, and the input to the channels will be x_h/h and x_w/w for the parallel and series channels respectively, and ρ_a will be expressed in multiples of ρ_c.

In Figure 3, the parallel and series storage capacity is shown as a function of σ. A practical interpretation of the meaning of σ is that it represents the standard deviation of the logarithm of ρ_a. In Figure 3, the series channels are represented as dashed red curves and the parallel channels as solid black curves. Several set of parameters are considered: $\mu \in \{\log 10, \log 100, \log 1000\}$ and $x_{\rm min} \in \{0.1, 0.05, 0.005\}$, with $x_{\rm max}$=0.5. The quantities $x_{\rm min}$ and $x_{\rm max}$ correspond to the minimum and maximum values of x_h and x_w in the series and parallel case, respectively. Within the considered set of parameters, the parallel channel has always a capacity at least 1.7 bits/cell greater than that of the series channel ($\mu = \log 10, x_{\rm min} = 0.1$). With a practical set of parameters, i.e., conservatively $\mu = \log 100, x_{\rm min} = 0.05$, this difference increases to 5 bits/cell. Note that in this and the following figures the position of markers in the figure is arbitrary and purely ment to help disinguish the curves. The bottom 3 red dashed curves refer to the series case and each actually

In Figure 4, a sensitivity analysis of capacity versus the minimum thickness (or width) of the amorphous material, $x_{\rm min}$, is shown. The set of parameters is as follows: $\mu \in \{\log 10, \log 100, \log 1000\}$ and $\sigma \in \{\log 1.1, \log 1.5, \log 2\} \simeq (0.095, 0.405, 0.693)$ (corresponding resistivity increases larger than 10%, 50%, and 100%, respectively, with probability 15.8%), and, $x_{\rm max}$=0.5.

The series and parallel channel are represented by red dashed and solid black curves, respectively. Again, the strongest factor influencing the capacity of the parallel channel is the parameter μ, i.e., the resistivity of the amorphous mate-

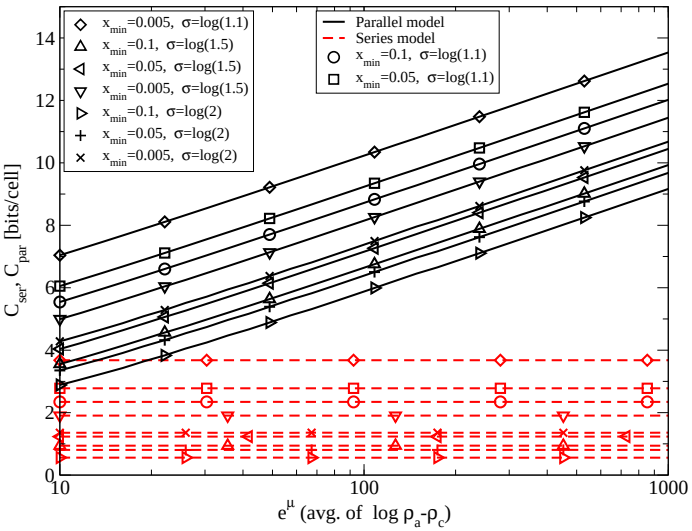

Fig. 5. Sensitivity of capacity versus amorphous material resistivity.

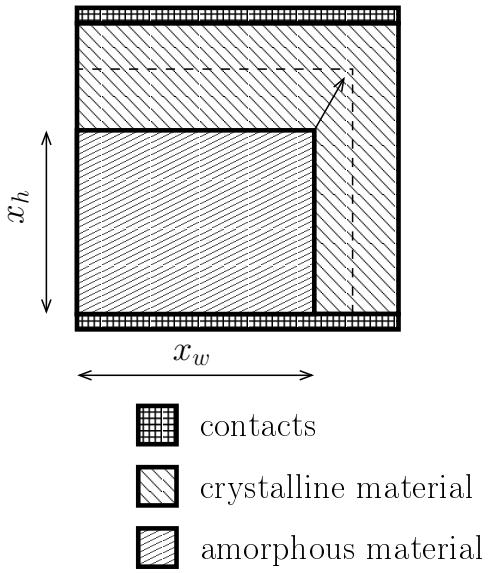

Fig. 6. Extended 2D model: the amorphous material can occupy any rectangular region with bottom left corner coinciding with the cell's bottom left corner.

rial. This parameter seems to have no influence on the capacity of the series channel, which in turn is influenced mostly by the noise As expected the dependence of the storage capacity on $x_{\min}$ is perceivable but not large. In particular, since the predicted increase in capacity is $\sim \log(\log x_{\max} - \log x_{\min})$, by interpreting $x_{\min}$ as a precision parameter (e.g., the minimum controllable thickness), it becomes clear that increasing the number of bits by extending precision of control of the amorphous material width is difficult (0.1 to 0.005 gives about 1.5 bits).

Proportionally, the capability of fine control of the amorphous material thickness is more relevant in the series configuration, where going from $x_{\min} = 0.1$ to $x_{\min} = 0.005$ almost doubles the storage capacity.

In Figure 5, the storage capacity versus e^{μ} is shown for a number of series and parallel configurations. From this figure it is easy to infer that the series channel storage capacity does not depend on the average resistivity of the amorphous material. The noise parameter σ and the minimum amorphous material thickness/width play a similar role in the considered range of parameters. The storage capacity of the parallel channel, on the other hand, exhibits a linear increase with μ.

Intuitively, the performance difference between the two structures is due to the fact that the resistance of the series cell is practically proportional to the amorphous material resistivity whereas, for large values of ρ_a the resistance of the parallel cell almost only depends on the geometry of the amorphous and crystalline shapes, thus making the output resistance less sensitive to noisy variations of the amorphous resistance.

V. A more general 2D model

So far, the amorphous material configurations that we considered could be described with a single parameter (i.e., x_h, or x_w). In order to obtain further insights on the relationship between the geometrical distribution of amorphous material and the storage capacity, we numerically investigate the storage capacity assuming a larger family of shapes for the amorphous material. In particular, we focus on the family of amorphous material shapes comprising all rectangles with one corner coinciding with the bottom left corner of the cell. This family is illustrated in Figure 6, where an example configuration is shown, with the relevant descriptive parameters. Each input shape is described by two parameters (x_h, x_w). This new family of amorphous shapes is particularly interesting since it comprises as subfamilies the series and the parallel configurations. In particular, the series configurations are those with $x_w = w$. The parallel configurations, strictly speaking, are those with $x_h = h$, however, we point out that all configurations with $x_w < w$ exhibit a conductive path form bottom to top electrode through the crystalline material.

In order to numerically estimate the capacity, we need to obtain the statistical relationship between the programmed amorphous material rectangle and the resistance of the memory cell. To this end, we use a finite difference approach for the computation of the resistance of the cell as a function of the amorphous material resistivity ρ_a. Given the distribution of ρ_a, this allows us to estimate the conditional pdf of the resistance, conditioned on the amorphous material shape, namely, given the width and height (x_w, x_h) of the amorphous material.

To evaluate the total resistance, the cell is decomposed in a uniform orthogonal grid, as shown in Figure 7. The cell surface is divided in squares, each either in the amorphous or in the crystalline state. Each square is then represented by a network of 4 resistors. The value of each resistor is half the sheet resistance (i.e., the surface resistivity) of the corresponding material, as illustrated in the bottom part of Figure 7.[2]

The resistivity value ρ_c is fixed equal to 1. For every pair

[2]The value of the resistors can be deduced from symmetry considerations and solving for the simple case where the material is uniform.

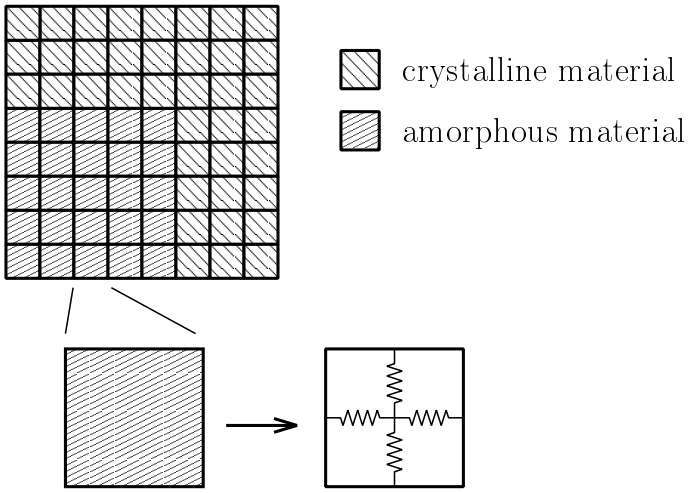

Fig. 7. Pictorial description of the finite difference method for resistive surfaces.

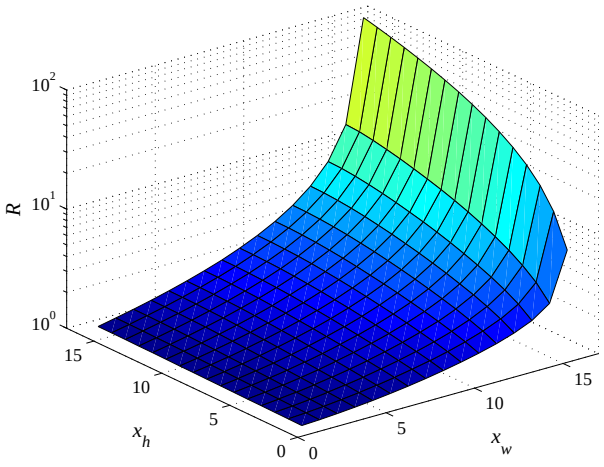

Fig. 8. Cell resistance as a function of the position of the top left corner of the amorphous material rectangle.

(x_h, x_w) we fix the contact voltages to 0 and 1, respectively, and, for several values of ρ_a, solve for the total current. By performing a fitting we obtain a functional representation of the total resistance R as a function of ρ_a, which in turn we use for numerically evaluating the resistance distribution conditioned to the written amorphous shape. In Figure 8, the cell resistance is shown as a function of the corner coordinates (x_w, x_h), assuming $\rho_a = 100$, $\rho_c = 16$, $h = w = 16$ and using 16 subdivisions for both width and height. The resistance steeply increases for x_w close to h. All parallel configurations except $(x_w, x_h) = (w, h)$ lay within one order of magnitude from the resistance of the cell in a completely crystalline state.

Using $h = w$ and a subdivision in a grid of 16 by 16 elements, $\mu = \log(100\rho_c)$, and $\sigma = \log(4)$, we compute estimates of capacity and optimal input distribution using the

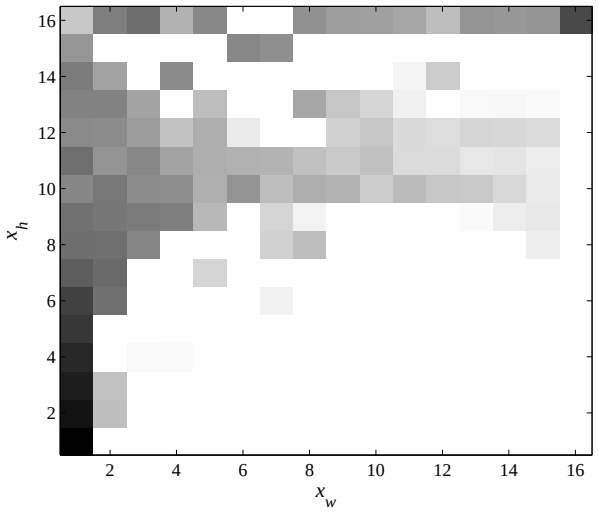

Fig. 9. 2D representation of the optimized probability mass function of the top left corner of the amorphous material rectangle.

Blahut-Arimoto (B-A) algorithm. Since increasing the number of grid subdivisions leads to a numerically intensive operation, the value of σ is kept large in order to operate in a region where a 16 by 16 grid subdivision is not the limiting factor of the capacity.

In Figure 9, a plot of the optimal input distribution for the top right corner of the amorphous rectangle is shown. Grid points are shown as squares whose color is the darker the higher the probability of the point. Even if the data set exhibits some noise (convergence of the input distribution in the B-A algorithm is typically very slow), the data set shows that no use is made of the series configurations (those for which $x_w = w$). The probability is mostly distributed in two configurations:

- the parallel configurations with a thick layer of amorphous material (i.e., the rectangle height being 50% or more of h)
- a thin vertical pillar of amorphous material ($x_w = 1$).

All series configurations except for the amorphous rectangle completely filling the cell, have a negligible probability.

The presence of the thin pillar is probably due to the fact that the resistance noise at these configurations is very small. A practical scheme, however will have to be able to distinguish between very small resistance differences to perceive the different programmed resistance values (see Figure 8 for $x_w = 1$),which probably makes the thin pillar points unpractical.

In Figure 10, the two-dimension cumulative mass function of the optimal input distribution is shown. This figure allows to better visualize the optimized input distribution from a quantitative point of view. Observe that the growth is concentrated on the borders $x_w = 1$, $x_h = 16$, and in the center region $x_h \geq 0.5h = 8$. The configurations with $x_h < 0.5h$ have a negligible probability. This is due to the fact that those configurations exhibit a larger noise, which can be attributed

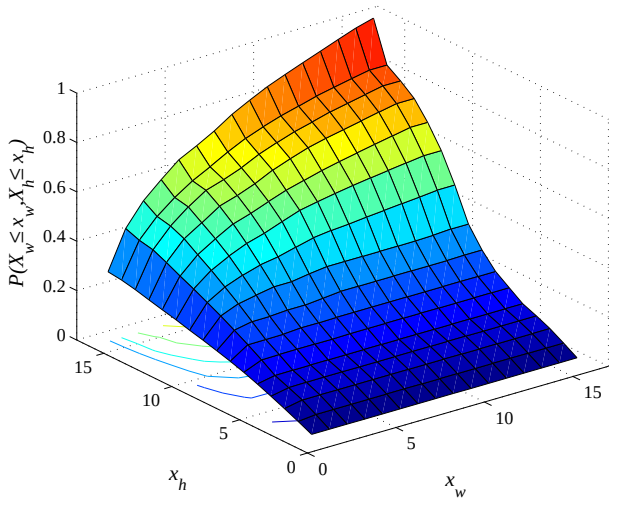

Fig. 10. Two-dimension cumulative mass function of the optimal distribution of the top left corner of the amorphous material rectangle.

to the fact that the amorphous material is thinner and a larger amount of current is passing through it, thus increasing the influence of the ρ_a on the total resistivity.

VI. Conclusions and Remarks

In this paper we analyze a simplified 2D PCM cell model in order to get insights on how the amorphous material should be distributed to maximize the storage capacity of the cell.

We consider two different cell paradigms, the *series model* and the *parallel model*, and show that each model can be interpreted through an equivalent additive channel model. Through numerical evaluation we demonstrate that the parallel structure has superior storage capacity, with gains ranging from 1.5 bits/cell to several bits per cell, depending on the operating conditions. In addition, we numerically obtain optimal input distributions for a broader cell model, which allow for configurations of the amorphous material that comprise as subclasses, the series and the parallel configurations. The results suggest that storage capacity is obtained using configurations that always allow for a parallel flow of current through crystalline material.

We remark that the storage capacity of real memory cells depends on a number of parameters, which might need to be estimated or can exhibit a stochastic behavior. Future work will try to extend the analysis accounting for a broader set of physical phenomena.

The approach of this paper and the results are an attempt to introduce information theory tools in the physical design of memory elements. We believe in fact, that modern memory cell design should take into account the stochastic nature of nanometer scale memory devices and the presence of advanced signal processing. This also implies for instance, that parameters that represent a cost, such as, programming energy, should also be considered in terms of cost per stored bit and not only as absolute values.

Acknowledgment

The authors wish to acknowledge Bipin Rajendran, Matt Breitwisch and Alan Bivens for the fruitful discussions.

References

[1] G. W. Burr *et al.*, "Phase change memory technology," *Journal of Vacuum Science and Technology*, April 2010, available on Arxiv.org.

[2] D.-H. Kang *et al.*, "Two-bit cell operation in diode-switch phase change memory cells with 90nm technology," in *Proc. VLSI'08*, Hyderabad, January 4-8 2008.

[3] T. Nirschl, J. B. Philipp, T. D. Happ, G. W. Burr, B. Rajendran, M. H. Lee, A. Schrott, M. Yang, M. Breitwisch, and C. F. Chen, "Write strategies for 2 and 4-bit multi-level phase-change memory," *IEEE International Electron Devices Meeting, 2007. IEDM 2007.*, pp. 461–464, 2007.

[4] F. Bedeschi, R. Fackenthal, C. Resta, E. M. Donze, M. Jagasivamani, E. Buda, F. Pellizzer, D. Chow, A. Cabrini, and G. M. A. Calvi, "A multi-level-cell bipolar-selected phase-change memory," *Solid-State Circuits Conference, 2008. ISSCC 2008. Digest of Technical Papers. IEEE International*, pp. 428–625, 2008.

[5] S. Lavizzari, D. Ielmini, D. Sharma, and A. Lacaita, "Reliability impact of Chalcogenide-Structure relaxation in Phase-Change memory (PCM) Cells–Part II: Physics-Based modeling," *Electron Devices, IEEE Transactions on*, vol. 56, no. 5, pp. 1078–1085, 2009.

[6] M. Franceschini, L. A. Lastras-Montaño, A. Jagmohan, M. Sharma, R. Cheek, and Ming-Hsiu Lee, "A communication-theoretic approach to phase change storage," in *International Conference on Communications (ICC 2010)*, Cape Town, South Africa, May 2010.

[7] L. A. Lastras-Montaño, M. Franceschini, T. Mittelholzer, and M. Sharma, "Rewritable storage channels," in *Proc. ISITA'08*, Auckland, New Zealand, 7th - 10th Dec. 2008.

[8] D. Ielmini, M. Boniardi, A. L. Lacaita, A. Redaelli, and A. Pirovano, "Unified mechanisms for structural relaxation and crystallization in phase-change memory devices," *Microelectronic Engineering*, vol. 86, no. 7-9, pp. 1942–1945, 2009.

[9] A. Redaelli, A. Pirovano, A. Locatelli, and F. Pellizzer, "Numerical implementation of low field resistance drift for phase change memory simulations," in *Non-Volatile Semiconductor Memory Workshop and International Conference on Memory Technology and Design. NVSMW/ICMTD 2008. Joint*, 2008, pp. 39–42.

[10] K. Sonoda *et al.*, "A Compact Model of Phase-Change Memory Based on Rate Equations of Crystallization and Amorphization," *IEEE Transactions on Electron Devices*, vol. 55, no. 7, pp. 1672–1660, Jul. 2008.

[11] L. A. Lastras-Montaño, T. Mittelholzer, and M. Franceschini, "Superposition coding in rewritable channels," in *Information Theory and Applications workshop (ITA2010)*, San Diego, CA, USA, 31st Jan. - 5th Feb. 2010.

[12] R. Blahut, "Computation of channel capacity and rate-distortion functions," *IEEE transactions on Information Theory*, vol. 18, no. 4, pp. 460–473, 1972.